PCCP

PAPER

View Article Online
View Journal | View Issue

Cite this: *Phys. Chem. Chem. Phys.*, 2014, **16**, 5553

Dissociative adsorption of 2,3,7,8-TCDD on the surfaces of typical metal oxides: a first-principles density functional theory study†

Shuo Zhao,[a] Xiaodong Ma,*[a] Qin Pang,[a] Hongwen Sun[a] and Guichang Wang*[b]

Received 29th November 2013,
Accepted 22nd January 2014

DOI: 10.1039/c3cp55048f

www.rsc.org/pccp

The initial dissociative adsorption step of the 2,3,7,8-tetrachlorodibenzo-*p*-dioxin (2,3,7,8-TCDD) molecule on the surfaces of MgO, CaO, and CuO has been studied by density functional theory (DFT) using periodic slab models. It is found that the 2,3,7,8-TCDD molecule undergoes a similar dissociative adsorption step during the decomposition over the three metal oxide surfaces. The adsorption configuration of 2,3,7,8-TCDD first converts from a parallel mode into a vertical one, then a nucleophilic substitution process takes place, where the surface oxygen atom attacks the aromatic carbon to form a surface phenolate with the chlorine atom moving to the top of the nearest surface metal atom. The calculated apparent activation energy of the dissociation increases in the order of CuO < CaO < MgO. The reaction heat is −0.67 eV, −0.75 eV, and 0.45 eV for CuO, CaO, and MgO, respectively, suggesting the thermodynamic tendency of MgO < CuO < CaO, which parallels the trend of the nucleophilicity of surface oxygen atoms. This study suggests that metal oxides with more nucleophilic and less tightly-bonded surface oxygen atoms might be more promising for the decomposition of polychlorinated dibenzo-*p*-dioxins and dibenzofurans.

1. Introduction

Polychlorinated dibenzo-*p*-dioxins and dibenzofurans (PCDD/Fs) resulting from the incineration of municipal and hazardous solid wastes are highly toxic, carcinogenic, and persistent organic pollutants.[1–3] Among the various strategies to reduce the emission of these substances, catalytic oxidation of PCDD/Fs to CO_x, H_2O and HCl has been demonstrated to be the most promising method in virtue of its high efficiency and low cost.[4–7] In the past few decades, the main catalysts studied for the catalytic oxidation of PCDD/Fs are alkaline earth metal oxides and transition metal oxides.[8–14] Although the catalytic performance of the above two kinds of metal oxides have been subjected to intensive studies, the mechanism for the catalytic oxidation of PCDD/Fs has not yet been clearly understood.

In the previous experimental research studies, PCDD/Fs are often replaced by model compounds, such as chlorobenzenes[4,9,15] and chlorophenols,[16,17] which are less toxic and more convenient for detection. However, as reported in several studies,[18–20] the catalytic performance and mechanism for these model compounds may not be consistent with those for PCDD/Fs due to the significant differences between their chemical structures. Furthermore, some important intermediates that formed during the process of the reactions might be too transient to be discernible by the experimental studies. For example, it is generally believed that the dissociative adsorption of polychlorinated aromatics on the surface of metal oxides follows the Mars van Krevelen (MvK) mechanism,[7,9] which begins with Cl abstraction, followed by oxidation of the remaining aromatic ring to produce partial and final oxidation products. It is widely accepted that the dechlorination is the initial and key step in the catalytic decomposition of PCDD/Fs over metal oxides.[4] However, the actual detailed reaction pathway of the dechlorination step has never been directly observed by any *in situ* characterization technologies.

Compared with traditional experimental research studies, theoretical simulation may provide a more accurate, efficient and safer method to clarify the mechanism of catalytic oxidation of PCDD/Fs over metal oxides. However, up to now, few theoretical research studies devoted to the relevant reaction mechanism have been reported.

Considering the reported high activities of alkaline earth metal oxides and transition metal oxides, in this paper, we perform density functional theory studies to understand the

[a] *Key Laboratory of Environmental Pollution Process and Standard, Ministry of Education, Tianjin Key Laboratory of Environmental Remediation and Pollution Control, College of Environmental Science and Engineering, Nankai University, Tianjin 300071, China. E-mail: maxd@nankai.edu.cn; Fax: +86 22 23501117*

[b] *Department of Chemistry and the Center of Theoretical Chemistry Study, Nankai University, Tianjin, 300071, China. E-mail: wangguichang@nankai.edu.cn; Fax: +86 22 23502458*

† Electronic supplementary information (ESI) available. See DOI: 10.1039/c3cp55048f

initial dechlorination step of the most toxic congener of PCDD/Fs, 2,3,7,8-tetrachlorodibenzo-*p*-dioxin (2,3,7,8-TCDD), on the surface of typical alkaline earth metal oxides MgO and CaO and a typical transition metal oxide CuO. The thermodynamics and kinetics of the initial dissociative adsorption are systematically investigated by theoretical calculations. This study is helpful to obtain deeper insights into the nature of the dissociative process of PCDD/Fs on the surfaces of typical metal oxides.

2. Computational methods

Geometry optimization and total energy calculations are carried out by using the Vienna Ab-initio Simulation Package (VASP).[21–24] The spin-polarized calculations are performed by using the generalized gradient approximation (GGA) for exchange and correlation as developed by Perdew and Wang (PW91).[25,26] The projector augmented wave method (PAW)[27,28] is used to describe the interaction of the valence electrons with the ion core. The electronic states are expanded in a plane wave basis with a kinetic cut-off energy of 315 eV, since when a cut-off energy of 400 eV is used, the adsorption energy of the 2,3,7,8-TCDD molecule in the flat mode on the MgO surface, whose structure is going to be further elaborated in later sections, changed by only 0.052 eV. This value can be later shown to be only 2.60%, a small fraction of the total energy span of the reaction on the MgO surface. And this value also constitutes only 7.54% and 4.68% of the difference in apparent activation energy between the MgO surface and the CaO and CuO surfaces respectively. Hence the cut-off energy used is sufficient in this study. The total energy is converged to an accuracy of 1.0×10^{-5} eV in the self-consistent-field calculation of the electronic structure, and the ionic positions for the stationary states on the potential energy surface are relaxed so that the forces on each ion is less than 0.035 eV Å^{-1}. The nudged elastic band (NEB) method is employed to locate the transition states, which are confirmed later by frequency analyses. A *k*-point grid with a $3 \times 3 \times 1$ Monkhorst–Pack mesh is chosen for sampling the Brillouine zone. Specifically, in order to improve the description of the strongly-correlated electrons in the Cu d-orbitals, the GGA + *U* approach developed by Dudarev *et al.*[29–32] is utilized. In this work we have used $U = 7.5$ eV and $J = 0.98$ eV, which have been shown to provide a good description of the electronic and magnetic structures of CuO.[33]

Cubic NaCl-type crystal structure is selected for MgO and CaO, with crystal constants of 4.21 Å[34] and 4.81 Å[35] respectively. A structure with C_2/c symmetry and lattice parameters 4.65, 3.41, and 5.11 Å and a β angle of 99.48° is used for CuO.[36] As depicted in Fig. 1, the most stable surface planes of the three metal oxides,[33,37] MgO(100), CaO(100), and Cu-terminated CuO(111), are modelled by P(6×6), P(6×6), and P(4×4) supercells comprising three atomic layers, which are able to accommodate the relatively large size of the 2,3,7,8-TCDD molecule without unrealistic large lateral interactions between the periodic image replicas. Particularly, the electronic structure of CuO(111) is optimized to the antiferromagnetic arrangements

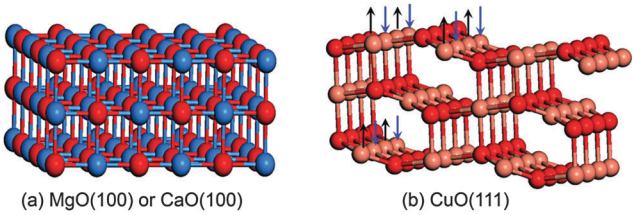

Fig. 1 (a) Geometries of the two alkaline earth metal oxides (ideal MgO(100) surface and CaO(100) surface). (b) Cu-terminated CuO(111) surface. Parts of the magnetic orderings of Cu atoms are depicted by arrows. O, Mg/Ca, and Cu are represented by red, blue, and pink spheres respectively.

of the localized spins. In the ionic coordinate relaxation, only the top layer is allowed to move with the bottom two layers fixed to mimic the surface of bulk crystals. And the three-layer model has been tested to be able to give satisfactory results for the adsorption energy of the 2,3,7,8-TCDD molecule. For instance, on the CaO surface, the adsorption energy of the 2,3,7,8-TCDD molecule just changed by 0.006 eV when a five-layer model is used. A vacuum thickness of at least 12 Å was employed to separate each slab from its neighbouring images along the *z*-direction, and the fictitious dipole–dipole interaction between slabs has been corrected out.

Due to the independence of the plane-wave basis from the system under study, the activation energy ΔE_a and the reaction heat ΔE are simply calculated as the difference in the energy of the transition state or the product with the reactant:

$$\Delta E_a = E_{TS} - E_{IS}$$

$$\Delta E = E_{FS} - E_{IS}$$

where IS denotes the initial state of the reaction, FS denotes the final state of the reaction and TS denotes the transition state of the reaction. Because of the size-extensivity and the size-consistency properties of the unrestricted density functional theory, the adsorption energy ΔE_{ADS} is simply calculated as the difference in the sum of the energy E_{surf} of the surface and the energy E_{mol} of the molecule with the energy E_{comp} of their composite system.

$$\Delta E_{ADS} = E_{comp} - E_{surf} - E_{mol}$$

3. Results and discussion

3.1 The dissociative adsorption of 2,3,7,8-TCDD on the MgO(100) surface

The reaction mechanism for the dissociative adsorption of the 2,3,7,8-TCDD molecule is first thoroughly studied on the least computationally-intensive MgO(100) surface.

3.1.1 Isolated 2,3,7,8-TCDD. The geometry of the 2,3,7,8-TCDD molecule optimized with our set-up of computational parameters is shown in Fig. 2 with important parameters listed in Table 1, along with previous crystallographic experimental results[38] and molecular DFT calculations at the level of theory

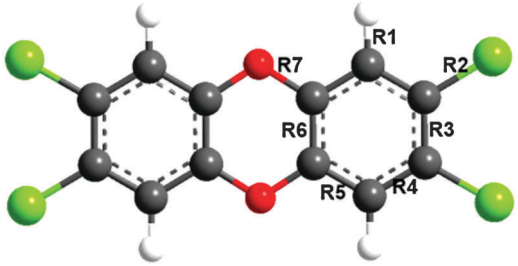

Fig. 2 Optimized structure of the 2,3,7,8-TCDD molecule. Bond distances in Å.

Table 1 Comparison of calculated bond lengths in the 2,3,7,8-TCDD molecule with previous theoretical and experimental values

Bond length	This study [Å]	Ref. 36 [Å]	Ref. 37 [Å]
R1	1.09	—	—
R2	1.73	1.743	1.727
R3	1.40	1.393	1.388
R4	1.40	1.392	1.384
R5	1.39	1.382	1.374
R6	1.40	1.393	1.386
R7	1.39	1.377	1.378

of B3LYP/6-311+G(2d,2p).[39] As can be seen from the comparison, our results are very close to the experimental values as well as theoretical values obtained by a method which is very suited for the geometry of organic molecules, showing the validity of our set-up for treating this molecule.

3.1.2 The non-dissociative adsorption of the 2,3,7,8-TCDD molecule. In order to find the most likely initial configuration for the dissociation of the 2,3,7,8-TCDD molecule, a lot of adsorption modes have been tested due to large numbers of possible orientations. All of these adsorption modes can be roughly categorized into three main categories: the ones with the molecule lying flat on the surface, the ones in which the aromatic plane of the molecule lies almost vertically to the surface with two C–Cl bonds pointing to the surface, and those with two C–H bonds pointing perpendicularly towards the surface. For each one of these three categories, 4–6 possible orientations have been tested. The most stable adsorption modes in each category are plotted in Fig. 3 with the energetic data summarized in Table 2. And the meta-stable configurations in each category are plotted in the ESI.† From these data it can be readily seen that the 2,3,7,8-TCDD molecule merely interacts with the MgO surface weakly by physisorption. And the potential energy surface tends to be very flat with many local minima of similar energy. Among all the modes, the one with the molecule lying parallel to the surface is the most stable one. So it is going to be considered to be the initial configuration for the dissociation and will be denoted by IS later on. And it has to be noted that the traditional density functional theory without either long-range-corrected hybrids[40] or specific van der Waals corrections[41] is not quite accurate in treating this weak interaction. So the physisorption energy obtained here might contain some inaccuracy. Nonetheless, all of these non-dissociative structures are thought to be weakly bound. As a result, as can be readily seen from later parts of this study, the contribution of this adsorption energy to the total evaluation of the activity of the metal oxides is very small when other parts are compared. So the reliability of the results of this study will not be limited by the incapability of DFT to treat weak interactions.

3.1.3 Adsorption of the products of the dissociation. In order to find the configuration of the system after the first dissociative dechlorination step, the adsorption of the two parts from the C–Cl bond dissociation, the chlorine atom and the 2,3,7-trichlorodibenzo-*p*-dioxin-8-yl moiety (later referred to as 2,3,7-TrCDD for short), is studied individually. Among all the adsorption positions for the chlorine atom, the bridge position has been found to be the most stable one, with an adsorption energy of −1.48 eV, which is 0.19, 0.24, and 0.02 eV higher than the hollow, top-Mg, and top-O positions respectively. For the 2,3,7-TrCDD moiety, these four adsorption positions are tested with both the aromatic plane perpendicular to and parallel to the surface. Not surprisingly, the perpendicular modes are found to be more stable, contrary to the case of molecular adsorption. This can be understood from the fact that the sp^2

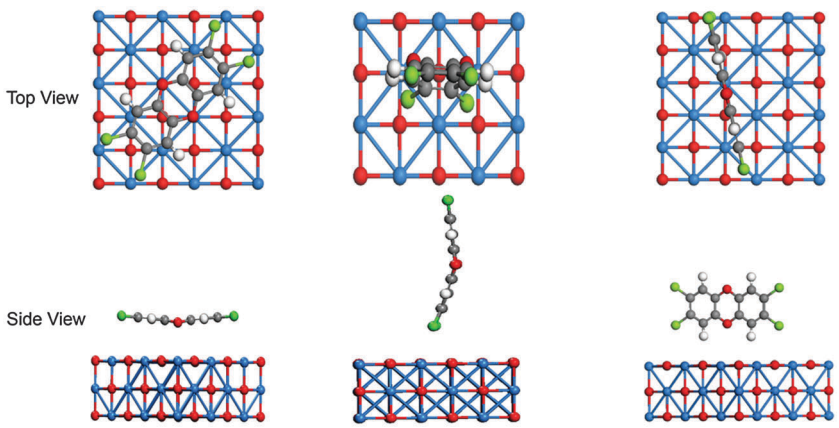

Fig. 3 The top and side views of the most stable orientation of every category of adsorption modes of the 2,3,7,8-TCDD molecule on the MgO(100) surface. Left: parallel configuration, middle: vertical configuration with C–Cl pointing down, and right: vertical configuration with C–H pointing down. Only parts of the atoms of the slab model are shown for clarity.

Table 2 The non-dissociative adsorption energy of the 2,3,7,8-TCDD molecule on the MgO surface in different adsorption modes. Vertical-1 and vertical-2 denote the vertical adsorption category with the C–Cl and C–H bond perpendicular to the surface respectively. Energies in eV

Orientation	Parallel [eV]	Vertical-1 [eV]	Vertical-2 [eV]
Most stable orientation	−0.29	−0.17	−0.15
Meta-stable orientation	−0.20, −0.18, −0.17	−0.10, −0.07, −0.03, −0.02, −0.01	−0.14, −0.10, −0.03, −0.01

Table 3 The adsorption energy of the 2,3,7-TrCDD moiety and the chlorine atom at various positions on MgO(100) in eV

Adsorbants	Bridge [eV]	Hollow [eV]	Top-Mg [eV]	Top-O [eV]
Cl	−1.48	−1.29	−1.24	−1.46
2,3,7-TrCDD-parallel	−0.25	−0.2	−0.25	−0.2
2,3,7-TrCDD-vertical	−0.53	−0.48	−0.53	−0.48

hybrid orbital on the fragment carbon atom can hardly achieve optimal overlap with any surface states when it is parallel to the surface. The 2,3,7-TrCDD moiety is found to be the most stable on the top of a magnesium atom, with the bridge position being just marginally less stable. The detailed adsorption energy data for all the adsorption modes are summarized in Table 3.

In the next step, the co-adsorption of one chlorine atom and 2,3,7-TrCDD is investigated to obtain the most stable configuration after the dissociation of the C–Cl bond. Initially, previous results regarding the different adsorption modes of the two individual parts were tried to be utilized. So the first co-adsorption configuration tested is one in which the chlorine atom is on a bridge position with 2,3,7-TrCDD residing on the top of a neighboring magnesium atom vertically. To some astonishment, this combination of the individually most stable adsorption modes just slipped into another configuration spontaneously in the optimization, where the chlorine atom got onto the top of a magnesium atom and 2,3,7-TrCDD moves onto the top of an oxygen atom forming a surface phenolate, finally giving a co-adsorption energy of −4.59 eV, which is 2.58 eV higher than the sum of the individual adsorption energies in their individual most stable adsorption positions (Cl – Bri, 2,3,7-TrCDD – Top-Mg) and 2.87 eV higher than the sum of the adsorption energies of the two parts in the same position as in this stable co-adsorption configuration (Cl – Top-Mg and 2,3,7-TrCDD – Top-O). Based on this strong tendency for 2,3,7-TrCDD to reside on top of an oxygen atom and the chlorine atom to go to a nearby magnesium atom when they are near to each other, other configurations with this arrangement but different orientations of 2,3,7-TrCDD have been tested, giving an co-adsorption energy of −1.50 eV when it is parallel to the surface and −4.22 eV when it is tilted. So the most stable vertical configuration is considered as the product state for the first dechlorination step, and will be addressed as FS later on. These configurations are pictorially shown in Fig. 4.

3.1.4 The activation energy of the C–Cl bond rupture. In order to really understand the kinetics of the first dechlorination step of the 2,3,7,8-TCDD molecule on the MgO surface, the transition state between the most stable initial configuration IS and the most stable final configuration FS is tried to be found. A string of sixteen image points are interpolated between them to start a NEB exploration of the potential energy surface. As can be expected from the long distance between IS and FS, the potential energy profile of this tentative NEB calculation does not render the simple bell shape of elementary reactions. An image point in the middle of the reaction coordinate goes into a locally minimum energy, indicating the presence of an intermediate along the minimum energy path. When an optimization toward potential energy minimum is performed for this locally minimum image point, the vertically adsorbed molecule with the C–Cl bond pointing toward the surface is obtained, which is 0.12 eV higher in energy than the most stable initial configuration. Then another NEB calculation is performed to locate the transition state between this vertical configuration and the final product, giving an activation energy of 1.88 eV. Since the first standing-up process does not require any bond breaking or formation, it can be expected that the energy of its transition state should be very similar to its final state, thus is certainly going to be lower than that of the C–Cl bond rupture step. So it has much less effect on the overall kinetics of the process. In this way, we can get the apparent activation energy, or energy span, between the two rate determining states[42,43] for the entire dissociation to be 2.00 eV, as shown in the potential energy profile in Fig. 5. This is quite consistent with the conjecture of Lichtenberger *et al.* that a perpendicular adsorption is required for the oxidation of dichlorobenzene on the vanadia–titania surface.[4] If the configuration with the vertically adsorbed intermediate is

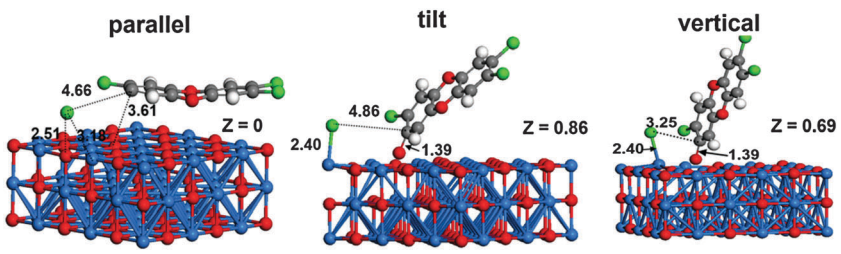

Fig. 4 The optimized structures for the three co-adsorption modes with different orientations of 2,3,7-TrCDD on the MgO(100) surface. Length in Å. "z" denotes the distance that the oxygen has moved up. Only parts of the atoms of the slab model are shown for clarity.

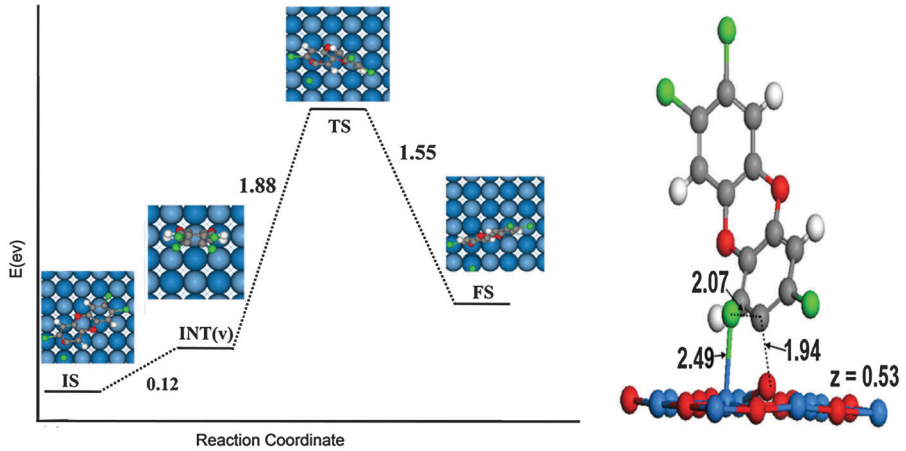

Fig. 5 The energy profile for the proposed dechlorination mechanism on the MgO(100) surface and the geometry parameters of the transition state (TS). Energies in eV and lengths in Å.

denoted by INT(v), the reaction pathway for the entire first dechlorination process can be written succinctly as IS-INT(v)-FS.

Now it can be seen that the dissociative adsorption of the 2,3,7,8-TCDD molecule on the MgO surface occurs *via* a two step mechanism. When the molecule just gets to the surface, most likely it will go into the position of lying parallel to the surface due to its low energy. For the dechlorination process to occur, it first needs to stand up to a meta-stable vertical adsorption mode before the C–Cl bond breaks. Then the chlorine atom goes to the top of a surface magnesium atom and 2,3,7-TrCDD forms surface phenolate with a nearby surface oxygen. This process is in good agreement with the nucleophilic substitution mechanism for dechlorination of dichlorobenzene on V_2O_5/TiO_2 catalysts proposed by Lichtenberger *et al.*[4] In order to further verify the nucleophilic substitution nature of this reaction step, a Bader charge analysis is performed on the vertical physisorption configuration.[44–46] With the atom serial numbers shown in Fig. 6 for the FS, the results are summarized in Table 4, where it can be quite apparently seen that electrons systematically move from the attacking oxygen atom (and the aromatic carbon)

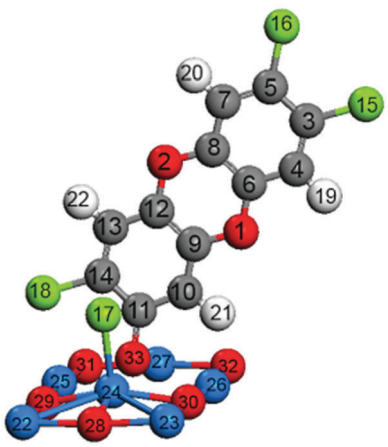

Fig. 6 The serial numbers for the atoms of FS on the MgO surface in the Bader charge analysis.

Table 4 The Bader charge of atoms near the reaction spot in the INT(v) and FS configurations. Atom serial numbers are shown in Fig. 6. Δe denotes the difference in charge between the dechlorinated product FS and the intermediate INT(v) before the dechlorination, positive values indicate the loss of electrons

Atom	$e_{INT(v)}$	e_{FS}	Δe	Atom	$e_{INT(v)}$	e_{FS}	Δe
C(11)	−0.02	0.32	0.34	Mg(26)	1.70	1.68	−0.02
Cl(17)	−0.19	−0.86	−0.67	O(29)	−1.68	−1.65	0.03
O(33)	−1.69	−1.38	0.31	O(31)	−1.67	−1.66	0.01
Mg(25)	1.70	1.67	−0.02	O(28)	−1.68	−1.66	0.02
Mg(24)	1.70	1.69	0.00	O(30)	−1.66	−1.66	0.00
Mg(27)	1.70	1.67	−0.03	O(32)	−1.68	−1.65	0.03

to the leaving chlorine atom, while the charge on all the other atoms remains mostly fixed. This is highly consistent with the nucleophilic substitution mechanism, where the oxygen should donate one unit of formal charge to the chlorine atom. And the change of the charge on the carbon atom, as well as the resulting inequality between the charge given by the oxygen atom and the charge received by the chlorine atom, can be easily understood from the greater electronegativity 3.44 of oxygen than the value 3.16 for chlorine.[47] If the process were to proceed by a homolytic cleavage of the C–Cl bond followed by individual adsorption of the two radicals, such systematic charge transfer would be highly unlikely. This nucleophilic substitution mechanism is also essentially the same as the first step of the nucleophilic elimination mechanism for the destructive adsorption of carbon tetraoxide on the lanthanide oxide surface.[48]

It is also interesting to note that the dechlorination by the nucleophilic attack of surface oxygen might be a very intricate synergistic process. Neither the chlorine nor the 2,3,7-TrCDD moiety from the dissociation is able to be very stably adsorbed on the surface. But when they are present together in near-by positions, the total stability of the system gets increased quite a lot. As a result, the leaving of the chlorine atom has to synchronize with the attacking of the surface oxygen atom to attain the lowest system energy, as can be seen from the transition state geometries. So the entire process can be shown

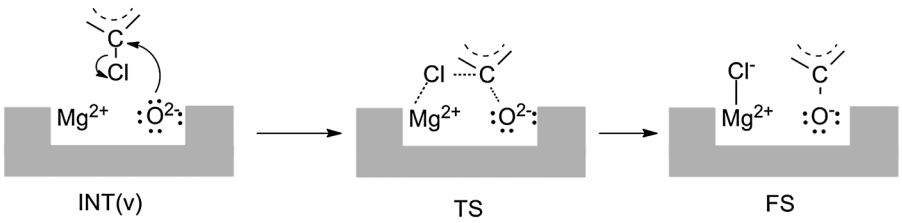

Fig. 7 Schematic for the nucleophilic substitution mechanism of the dechlorination process. The lone pairs of electrons on the oxygen atom are shown, and the arrows indicate the movement of the electron pairs.

schematically as in Fig. 7, which is essentially the same as the mechanism proposed by Khaleel *et al.* for the decomposition of chlorobenzene on iron and titanium oxide surfaces.[49] And this mechanism is highly consistent with the mechanism proposed by Lichtenberger *et al.* for the dechlorination of several different kinds of chlorinated benzene on V_2O_5/TiO_2 catalysts.[4] In this way, it can be seen that although the catalytic performance and the whole decomposition mechanism of chlorinated model compounds over metal oxides may not be consistent with those of PCDD/Fs,[4] combining this study and previous reports, it can be deduced that chlorinated aromatics may have a similar reaction pathway in their initial step of the dissociative adsorption process: the nucleophilic substitution mechanism.

3.2 The dissociative adsorption of 2,3,7,8-TCDD on CaO(100) and CuO(111) surfaces

3.2.1 Adsorption of the reactants and products of the dissociative process. The adsorption modes of the reactants and products of the initial dissociative process of 2,3,7,8-TCDD on CaO(100) and CuO(111) surfaces were also investigated. The extensive testing has also been performed without any simplification. First, several different orientations of the vertical and parallel adsorption of the 2,3,7,8-TCDD molecule had been tested, with the results summarized in Table 5, and configurations shown in Fig. 8. It can be seen that the adsorption energy all follows the same trend that the molecule lying parallel to the surface is energetically more favorable than standing-up vertically. And the energy difference between the most stable horizontal adsorption mode and the most stable vertical adsorption mode all falls within the 0.12–0.17 eV range.

For the configuration after the dissociation, co-adsorption modes with 2,3,7-TrCDD lying vertically, flatly, and tilted on a surface oxygen atom are all tested with a chlorine atom on top of a nearby magnesium atom. The results for the co-adsorption energy are shown in Table 6. Exactly the same case as on the MgO surface, the stability follows the trend of vertical > tilted > parallel. Now we can see that the most stable adsorption energy for the 2,3,7,8-TCDD molecule on the three surfaces increases in the order of CuO < CaO < MgO, and the co-adsorption energy of the products of the dissociative adsorption has the order of MgO < CuO < CaO. The product structures are shown in Fig. 9.

Despite the quantitative difference among the three surfaces, the relative order of the energy of different adsorption orientations of both the reactant and the product follows exactly the same trend on all three surfaces. The dioxin molecule is most stable when being parallel to the surface, while the dissociated product is most stable when being perpendicular to the surface. So it is highly likely that the same problem is going to be resolved in the same fashion on all the surfaces. In light of this, the transition states between the vertically-adsorbed 2,3,7,8-TCDD and the products of the dissociation are tried to be found by using the NEB method. This process is confirmed based on the energy landscape along the reaction coordinate, thus corroborating the validity of the mechanism. In fact this makes a lot of sense since the standing-up before the substitution mechanism is not only the calculated result but also a mechanism that is logical, given the contradiction between the most stable adsorption configuration of the reactants and the products. The 2,3,7,8-TCDD molecule is most stable when being adsorbed flatly on the surface to maximize the contact with the surface to get larger van der Waals interaction, while the substituted product is most stable when being perpendicular to the surface for maximal overlap of the sp^3 orbit with the surface states. The deviation of the reactant from its most stable configuration is not going to lead to a high energy penalty, since it is weak van der Waals interaction, while the deviation of the product from its most stable configuration will lead to a relatively larger energetic penalty, since it involves puckering a covalent bond. So it is reasonable to propose that the 2,3,7,8-TCDD molecule undergoes a similar dissociative adsorption step over three metal oxide surfaces: the 2,3,7,8-TCDD molecule would first pay a small energy penalty to stand up, and then it can go to the most stable configuration of the product directly after the substitution.

The configurations of the transition states and the energy profiles of the reaction on CaO and CuO surfaces are plotted in Fig. 10. The activation energy of this step is 1.15 and 0.71 eV on the CaO and CuO surfaces respectively. And it is interesting to

Table 5 Geometric parameters and adsorption energy for the most stable configuration of the 2,3,7,8-TCDD molecule parallel and vertical to the MgO(100), CaO(100) and CuO(111) surfaces. The D_{Cl-M} and D_{Cl-O} are the distances of the chlorine atom with its nearest magnesium and oxygen atoms. D_{C-Cl} is the C–Cl bond length

Surface	Configuration	E_{ads} [eV]	D_{C-Cl} [Å]	D_{Cl-M} [Å]	D_{Cl-O} [Å]
MgO(100)	Parallel	−0.29	1.73	3.64	3.90
	Vertical	−0.17	1.73	3.11	3.26
CaO(100)	Parallel	−0.26	1.73	2.79	2.87
	Vertical	−0.10	1.74	3.35	3.29
CuO(111)	Parallel	−0.22	1.72	3.84	3.53
	Vertical	−0.05	1.73	2.76	3.29

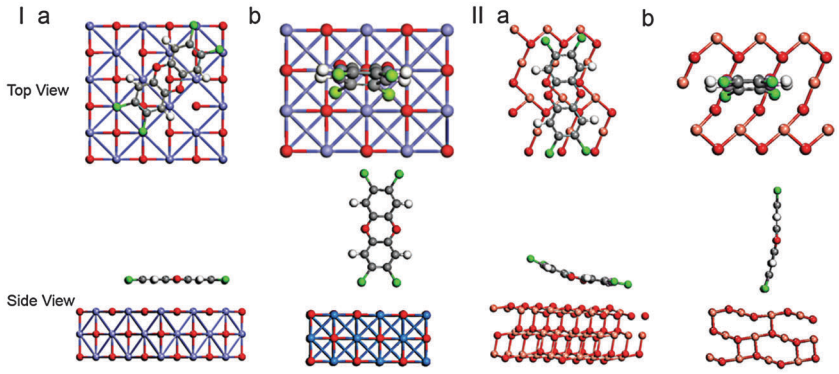

Fig. 8 The structures of the 2,3,7,8-TCDD molecule on the CaO(100) and CuO(111) surfaces. I-a and I-b for CaO and II-a and II-b for CuO. The atoms of the slab surface model are only partially shown for clarity.

Table 6 The co-adsorption energy of the products with different orientations of the aromatic plane in eV. The numbers in the parentheses are the energy differences in the most stable vertical mode

Orientation	MgO(100) [eV]	CaO(100) [eV]	CuO(111) [eV]
Parallel	−1.50 (3.09)	−2.52 (3.42)	−2.46 (3.38)
Tilted	−4.22 (0.37)	−5.40 (0.54)	−5.38 (0.46)
Vertical	−4.59 (0)	−5.95 (0)	−5.84 (0)

note that some important geometric factors in the transition state, like the distance between the leaving chlorine atom and its target metal atom, the elongated bond length of the C–Cl bond, and the distance between the attacking oxygen atom and the aromatic carbon, are very similar on the three surfaces: the above three distances are 2.49, 2.09, and 1.94 Å on the MgO surface, 2.79, 1.67, and 1.92 Å on the CaO surface, and 3.10, 2.29, and 1.90 Å on the CuO surface. This can be considered to be a corroboration for the 2,3,7,8-TCDD molecule following the same synergic mechanism shown in Fig. 7. The apparent activation energy, as defined as the energy difference between the transition state and the initial state of the reaction, will be 2.00 eV on the MgO surface, 1.31 eV on the CaO surface, and 0.89 eV on the CuO surface. And the total reaction heat will be 0.45 eV on the MgO surface, −0.75 eV on the CaO surface, and −0.67 eV on the CuO surface. So, kinetically, the rates for the dissociation would follow the order of MgO < CaO < CuO, while the thermodynamic tendency for the dissociation will be in the order of MgO < CuO < CaO. This is consistent with the experimental finding of the better performance of CaO and CuO over MgO.[50] This consistency also corroborates the correctness of the reaction pathway used in this study.

In order to understand the difference in the activity of the three different kinds of metal oxides, based on the nucleophilic mechanism of the reaction, it can be conjectured that greater nucleophilicity of the surface oxygen atom would facilitate this process. In order to verify this conjecture, the adsorption energy of a typical electrophile, CO_2,[51] on the surfaces has been calculated, giving an adsorption energy of −0.10 eV for MgO, −1.34 eV for CaO, and −0.47 eV for CuO. This trend MgO < CuO < CaO of the affinity toward the electrophilic CO_2 molecule exactly parallels the thermodynamic trend of the reaction, corroborating the above conjecture. At the same time, it needs to be noted that the kinetic trend differs from the above thermodynamic trend. This deviation from the common Brønsted–Evans–Polanyi relation[52] makes the problem unable to be easily understood.

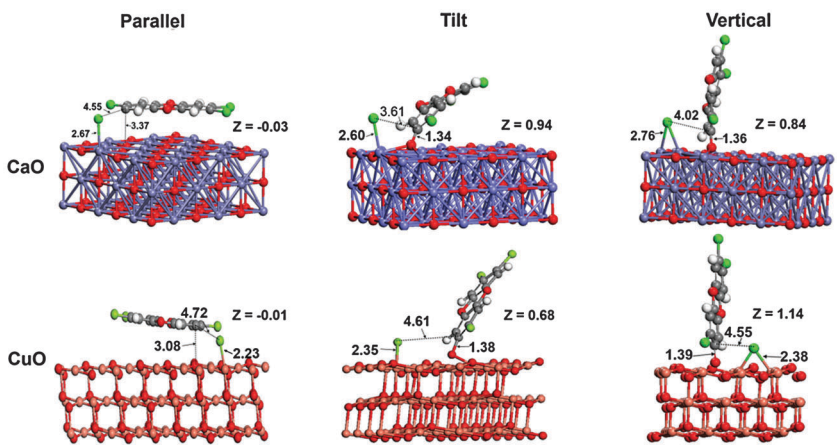

Fig. 9 The structures of the parallel, tilted and vertical orientations of 2,3,7-TrCDD on the CaO(100) and CuO(111) surfaces. Length in Å. "z" denotes the distance that the oxygen has moved up. The atoms of the slab model are only partially shown for clarity.

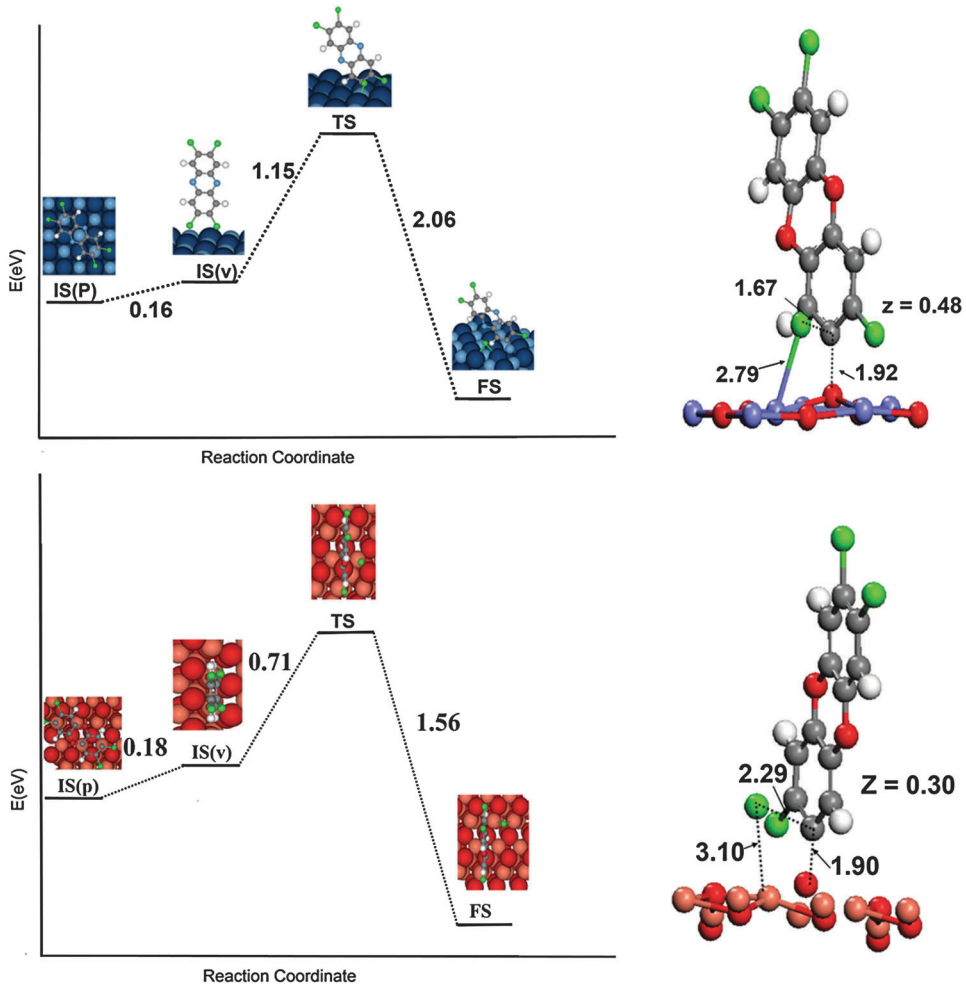

Fig. 10 The energy profile for the proposed dechlorination mechanism on the CaO(100) and CuO(111) surfaces and the geometry parameters of the transition state (TS). Energies in eV and lengths in Å.

But it is interesting to note that the force constant for a surface oxygen moving up in the z direction, *i.e.* the Hessian matrix element in the diagonal position of the z-direction of a surface oxygen atom, goes as 6.86 eV Å^{-2} for MgO, 4.50 eV Å^{-2} for CaO, and 0.28 eV Å^{-2} for CuO, which exactly parallels the kinetic trend of the three oxides. So probably the less steep potential energy surface of CuO locally around its equilibrium position makes its transition to another position easier with a lower energy barrier, although generally the process is more energetically favorable on the CaO surface. It can be deduced that oxides with more nucleophilic and more loosely-bound surface oxygen atom might be more promising for the dissociative adsorption of polychlorinated dibenzo-*p*-dioxins and dibenzofurans.

4. Conclusion

In this study, the first dissociative adsorption step of the dechlorination of the 2,3,7,8-TCDD molecule is thoroughly studied on the MgO(100), CaO(100), and CuO(110) surfaces. The molecule is found to be most stable when it is adsorbed flatly. But 2,3,7-TrCDD from the dissociation is most stable when standing vertically on a surface oxygen atom forming a surface phenolate. The process proceeds *via* a two-step mechanism: the molecule first stands up in a meta-stable vertical adsorption mode, and then the surface oxygen atom attacks the aromatic ring nucleophilically. The chlorine atom is found to move synergistically to the top of a nearby surface metal atom. The nucleophilic substitution nature of the reaction has been verified by Bader charge analysis, and is consistent with the dechlorination mechanism conjectured in several experimental studies on the decomposition of surrogate chlorinated aromatic compounds. The apparent activation energy follows the order of CuO < CaO < MgO. And the thermodynamic tendency obeys the sequence of MgO < CuO < CaO, which is exactly the same as the order of the nucleophilicity of the surface oxygen atom (as measured by the adsorption energy of a CO_2 molecule on a surface oxygen atom). This consistency corroborates the validity of the mechanism and it can be expected that metal oxide surfaces with more nucleophilic and less tightly-bonded surface oxygen atoms might be more active for this process.

Acknowledgements

The authors gratefully acknowledge financial support from National Natural Science Foundation of China (No. 21177066, 41225014 and 31370700), the Science and Technology Commission Foundation of Tianjin (No. 11JCYBJC05100), and Program for New Century Excellent Talents in University (NCET-12-0284).

References

1 L. P. Brzuzy and R. A. Hites, Global mass balance for polychlorinated dibenzo-p-dioxins and dibenzofurans, *Environ. Sci. Technol.*, 1996, **30**, 1797–1804.
2 V. P. Santos, M. F. Pereira, J. J. Orfao and J. L. Figueiredo, Mixture effects during the oxidation of toluene, ethyl acetate and ethanol over a cryptomelane catalyst, *J. Hazard. Mater.*, 2011, **185**, 1236–1240.
3 X. Ma, X. Feng, J. Guo, H. Cao, X. Suo, H. Sun and M. Zheng, Catalytic oxidation of 1,2-dichlorobenzene over Ca-doped FeO_x hollow microspheres, *Appl. Catal., B*, 2014, **147**, 666–676.
4 J. Lichtenberger and M. D. Amiridis, Catalytic oxidation of chlorinated benzenes over V_2O_5/TiO_2 catalysts, *J. Catal.*, 2004, **223**, 296–308.
5 X. Gao, W. Wang and X. Liu, Dechlorination reaction of hexachlorobenzene with calcium oxide at 300–400 °C, *J. Hazard. Mater.*, 2009, **169**, 279–284.
6 X. Ma, X. Feng, X. He, H. Guo, L. Lv, J. Guo, H. Cao and T. Zhou, Mesoporous CuO/CeO_2 bimetal oxides: One-pot synthesis, characterization and their application in catalytic destruction of 1,2-dichlorobenzene, *Microporous Mesoporous Mater.*, 2012, **158**, 214–218.
7 X. Ma, Q. Sun, X. Feng, X. He, J. Guo, H. Sun and H. Cao, Catalytic oxidation of 1,2-dichlorobenzene over $CaCO_3/\alpha$-Fe_2O_3 nanocomposite catalysts, *Appl. Catal., A*, 2013, **450**, 143–151.
8 S. P. Decker, J. S. Klabunde, A. Khaleel and K. J. Klabunde, Catalyzed destructive adsorption of environmental toxins with nanocrystalline metal oxides. Fluoro-, chloro-, bromo-carbons, sulfur, and organophosophorus compounds, *Environ. Sci. Technol.*, 2002, **36**, 762–768.
9 X. Ma, J. Shen, W. Pu, H. Sun, Q. Pang, J. Guo, T. Zhou and H. Cao, Water-resistant Fe-Ca-O_x/TiO_2 catalysts for low temperature 1,2-dichlorobenzene oxidation, *Appl. Catal., A*, 2013, **466**, 68–76.
10 P. H. Ruokojärvi, I. A. Halonen, K. A. Tuppurainen, J. Tarhanen and J. Ruuskanen, Effect of gaseous inhibitors on PCDD/F formation, *Environ. Sci. Technol.*, 1998, **32**, 3099–3103.
11 R. Weber, T. Sakurai and H. Hagenmaier, Low temperature decomposition of PCDD/PCDF, chlorobenzenes and PAHs by TiO_2-based V_2O_5-WO_3 catalysts, *Appl. Catal., B*, 1999, **20**, 249–256.
12 X. Ma, H. Sun, Q. Sun, X. Feng, H. Guo, B. Fan, S. Zhao, X. He and L. Lv, Catalytic oxidation of CO and *o*-DCB over CuO/CeO_2 catalysts supported on hierarchically porous silica, *Catal. Commun.*, 2011, **12**, 426–430.
13 S. Lin, G. Su, M. Zheng, M. Jia, C. Qi and W. Li, The degradation of 1,2,4-trichlorobenzene using synthesized Co_3O_4 and the hypothesized mechanism, *J. Hazard. Mater.*, 2011, **192**, 1697–1704.
14 L. Huang, G. Su, A. Zhang, Y. Shi, C. Xia, H. Lu, L. Li, S. Liu and M. Zheng, Degradation of polychlorinated biphenyls using mesoporous iron-based spinels, *J. Hazard. Mater.*, 2013, **261**, 451–462.
15 S. Krishnamoorthy, Catalytic oxidation of 1,2-dichlorobenzene over supported transition metal oxides, *J. Catal.*, 2000, **193**, 264–272.
16 S. Lomnicki, J. Lichtenberger, Z. Xu, M. Waters, J. Kosman and M. D. Amiridis, Catalytic oxidation of 2,4,6-trichlorophenol over vanadia/titania-based catalysts, *Appl. Catal., B*, 2003, **46**, 105–119.
17 C. E. Hetrick, J. Lichtenberger and M. D. Amiridis, Catalytic oxidation of chlorophenol over V_2O_5/TiO_2 catalysts, *Appl. Catal., B*, 2008, **77**, 255–263.
18 J. Lee and J. Jurng, Catalytic conversions of polychlorinated benzenes and dioxins with low-chlorine using V_2O_5/TiO_2, *Catal. Lett.*, 2008, **120**, 294–298.
19 D. P. Debecker, R. Delaigle, P. C. Hung, A. Buekens, E. M. Gaigneaux and M. B. Chang, Evaluation of PCDD/F oxidation catalysts: confronting studies on model molecules with tests on PCDD/F-containing gas stream, *Chemosphere*, 2011, **82**, 1337–1342.
20 D. P. Debecker, F. Bertinchamps, N. Blangenois, P. Eloy and E. M. Gaigneaux, On the impact of the choice of model VOC in the evaluation of V-based catalysts for the total oxidation of dioxins: Furan *vs.* chlorobenzene, *Appl. Catal., B*, 2007, **74**, 223–232.
21 G. Kresse and J. Furthmüller, Efficiency of ab-initio total energy calculations for metals and semiconductors using a plane-wave basis set, *Comput. Mater. Sci.*, 1996, **6**, 15–50.
22 G. Kresse and J. Furthmüller, Efficient iterative schemes for ab initio total-energy calculations using a plane-wave basis set, *Phys. Rev. B: Condens. Matter Mater. Phys.*, 1996, **54**, 11169–11186.
23 G. Kresse and J. Hafner, Ab initio molecular dynamics for liquid metals, *Phys. Rev. B: Condens. Matter Mater. Phys.*, 1993, **47**, 558–561.
24 G. Kresse and J. Hafner, Ab initio molecular-dynamics simulation of the liquid-metal–amorphous-semiconductor transition in germanium, *Phys. Rev. B: Condens. Matter Mater. Phys.*, 1994, **49**, 14251–14269.
25 J. P. Perdew, J. A. Chevary, S. H. Vosko, K. A. Jackson, M. R. Pederson, D. J. Singh and C. Fiolhais, Atoms, molecules, solids, and surfaces: applications of the generalized gradient approximation for exchange and correlation, *Phys. Rev. B: Condens. Matter Mater. Phys.*, 1992, **46**, 6671–6687.
26 J. P. Perdew and Y. Wang, Accurate and simple density functional for the electronic exchange energy: Generalized gradient approximation, *Phys. Rev. B: Condens. Matter Mater. Phys.*, 1986, **33**, 8800–8802.
27 P. E. Blöchl, Projector augmented-wave method, *Phys. Rev. B: Condens. Matter Mater. Phys.*, 1994, **50**, 17953–17979.

28 G. Kresse and D. Joubert, From ultrasoft pseudopotentials to the projector augmented-wave method, *Phys. Rev. B: Condens. Matter Mater. Phys.*, 1999, **59**, 1758–1775.
29 V. I. Anisimov, J. Zaanen and O. K. Andersen, Band theory and Mott insulators: Hubbard *U* instead of Stoner *I*, *Phys. Rev. B: Condens. Matter Mater. Phys.*, 1991, **44**, 943–954.
30 V. I. Anisimov, *et al.*, First-principles calculations of the electronic structure and spectra of strongly correlated systems: the LDA+U method, *J. Phys.: Condens. Matter*, 1997, **9**, 767–808.
31 D. Wu, Q. Zhang and M. Tao, LSDA+U study of cupric oxide: Electronic structure and native point defects, *Phys. Rev. B: Condens. Matter Mater. Phys.*, 2006, **73**, 235206.
32 S. L. Dudarev, G. A. Botton, S. Y. Savrasov, C. J. Humphreys and A. P. Sutton, Electron-energy-loss spectra and the structural stability of nickel oxide: An LSDA+U study, *Phys. Rev. B: Condens. Matter Mater. Phys.*, 1998, **57**, 1505–1509.
33 J. Hu, D. Li, J. G. Lu and R. Wu, Effects on electronic properties of molecule adsorption on CuO surfaces and nanowires, *J. Phys. Chem. C*, 2010, **114**, 17120–17126.
34 D. Taylor, Thermal expansion data. I. binary oxides with the sodium chloride and wurtzite structure, *Br. Ceram. Trans. J.*, 1984, **83**, 5–9.
35 M. C. Verbraeken, E. Suard and J. T. S. Irvine, Structural and electrical properties of calcium and strontium hydrides, *J. Mater. Chem.*, 2009, **19**, 2766–2770.
36 G. Tunell, E. Posnjak and C. J. Ksanda, Geometrical and optical properties, and crystal structure of tenorite, *Z. Kristallogr. Krist.*, 1935, **90**, 120–142.
37 M. Calatayud, Ethylene glycol interaction on alkaline earth oxides: a periodic DFT study, *Catal. Today*, 2010, **152**, 88–92.
38 A. W. Cordes and C. K. Fair, Dibenzo-p-dioxin, *Acta Crystallogr., Sect. B: Struct. Sci.*, 1974, **30**, 1621–1623.
39 Y.-Y. Zhao, F.-M. Tao and E. Y. Zeng, Structures, reductive dechlorination, and electron affinities of selected polychlorinated dibenzo-p-dioxins: density functional theory study, *J. Phys. Chem. A*, 2007, **111**, 11638–11644.
40 R. M. Irelan, T. M. Henderson and G. E. Scuseria, Long-range-corrected hybrids using a range-separated Perdew–Burke–Ernzerhof functional and random phase approximation correlation, *J. Chem. Phys.*, 2011, **135**, 094105.
41 S. Grimme, Accurate description of van der Waals complexes by density functional theory including empirical corrections, *J. Comput. Chem.*, 2004, **25**, 1463–1473.
42 S. Kozuch and S. Shaik, How to conceptualize catalytic cycles? The energetic span model, *Acc. Chem. Res.*, 2010, **44**, 101–110.
43 S. Kozuch and J. M. L. Martin, The rate-determining step is dead. Long live the rate-determining state!, *ChemPhysChem*, 2011, **12**, 1413–1418.
44 W. Tang, E. Sanville and G. Henkelman, A grid-based Bader analysis algorithm without lattice bias, *J. Phys.: Condens. Matter*, 2009, **21**, 084204.
45 E. Sanville, S. D. Kenny, R. Smith and G. Henkelman, Improved grid-based algorithm for Bader charge allocation, *J. Comput. Chem.*, 2007, **28**, 899–908.
46 G. Henkelman, A. Arnaldsson and H. Jónsson, A fast and robust algorithm for Bader decomposition of charge density, *Comput. Mater. Sci.*, 2006, **36**, 354–360.
47 *CRC Handbook of Chemistry and Physics*, ed. D. R. Lide, CRC Press, Boca Raton, Florida, 84 edn, 2003.
48 P. Van der Avert, S. G. Podkolzin, O. Manoilova, H. de Winne and B. M. Weckhuysen, Low-temperature destruction of carbon tetrachloride over lanthanide oxide-based catalysts: from destructive adsorption to a catalytic reaction cycle, *Chem.–Eur. J.*, 2004, **10**, 1637–1646.
49 A. Khaleel and A. Al-Nayli, Supported and mixed oxide catalysts based on iron and titanium for the oxidative decomposition of chlorobenzene, *Appl. Catal., B*, 2008, **80**, 176–184.
50 Y.-X. Li, H. Li and K. J. Klabunde, Destructive adsorption of chlorinated benzenes on ultrafine (nanoscale) particles of magnesium oxide and calcium oxide, *Environ. Sci. Technol.*, 1994, **28**, 1248–1253.
51 G. Pacchioni, J. M. Ricart and F. Illas, Ab-initio cluster model calculations on the chemisorption of CO_2 and SO_2 probe molecules on MgO and CaO(100) Surfaces. A theoretical measure of oxide basicity, *J. Am. Chem. Soc.*, 1994, **116**, 10152–10158.
52 T. Bligaard, J. K. Nørskov, S. Dahl, J. Matthiesen, C. H. Christensen and J. Sehested, The Brønsted–Evans–Polanyi relation and the volcano curve in heterogeneous catalysis, *J. Catal.*, 2004, **224**, 206–217.

